2007-4197

18th AIAA Computational Fluid Dynamics Conference, 25–28 June 2007, Miami FL

Evaluation of Traditional and Shock-Confining LES Filters using DNS Data of Compressible Turbulence

Ellen M. Taylor,* Nathan E. Grube,* and M. Pino Martín†

Princeton University, Princeton NJ 08544

Uniformly high-order-accurate filtering of fluid flow properties in the presence of shocks and shocklets is theoretically susceptible to the same problem that afflicts uniformly high-order-accurate numerical methods for approximating the convective terms of the Navier-Stokes equations: the introduction of new, non-physical extrema near discontinuities. Extensive investigations have been conducted into myriad types of shock-capturing methods, which adaptively decrease their order of accuracy within shock-containing regions in order to maintain accuracy and stability over time. Inspired by such work, Grube et al. (AIAA 2007-4198) have proposed the conceptually similar idea of "shock-confining" filtering (SCF) for compressible large-eddy simulations (LES), in which a class of linear filters is subject to adaptive adjustments based on smoothness information provided by a weighted essentially non-oscillatory (WENO) method. In the current work, we utilize the turbulent flow fields produced by direct numerical simulations (DNS) of shock/isotropic-turbulence interaction to perform preliminary *a priori* testing of these shock-confining filters against the corresponding linear filters. Although additional study, both *a priori* and *a posteriori*, is required to verify the necessity and suitability of SCF for LES, we conclude that linear filtering can indeed create serious qualitative discrepancies in global flow characteristics, discrepancies that are avoided by the use of SCF.

I. Introduction

The presence of shock waves in compressible fluid flow has long been known to elicit the creation of new, non-physical extrema known as Gibbs oscillations when uniformly high-order-accurate numerical methods are employed to approximate the spatial derivatives of the convective terms of the Navier-Stokes equations. These oscillations often grow with time, progressively corrupting the flow solution into uselessness. In turbulent flow, corrective low-pass filtering is likely to unacceptably degrade many of the natural turbulent fluctuations; therefore a sizable collection of high-order-accurate shock-capturing methods, including MUSCL,[1] TVD,[2,3] ENO,[4,5] and WENO[6,7] schemes, have been developed to avoid spurious oscillations by adaptively preventing high-order-accurate interpolation across discontinuities. In large-eddy simulations (LES), evaluation of the subgrid-scale (SGS) contributions to the momentum and energy transport mechanisms requires filtering operations that are mathematically similar to the finite-difference approximations incorporated by shock-capturing schemes. Thus these filters may in theory also generate Gibbs oscillations if uniformly applied in compressible flow.

With the exception of static eddy viscosity models, most turbulence models employed in the LES of flows of current engineering interest require the explicit application of filtering operations, sometimes more than once during a given time advancement stage. Dynamic,[8,9] scale-similarity,[10] and mixed[11,12] models rely on filtering to identify the smallest resolved length scales; and the approximate deconvolution model[13] relies on the iterative application of filtering to approximately de-filter the flow solution. Therefore the calculations of the unclosed terms of the filtered Navier-Stokes equations, and in turn the global dynamics of the simulated fluid flow, are directly affected by the choice of filtering technique. In a paper concurrent to this one, Grube et al.[14] propose a "shock-confining" filtering (SCF) approach for LES of compressible flow, in which a class

*Ph.D. Student, Department of Mechanical and Aerospace Engineering. AIAA Student Member.

†Assistant Professor, Department of Mechanical and Aerospace Engineering. AIAA Senior Member.

of commutative linear filters developed by Vasilyev et al.[15] is subject to adaptive adjustments based on flow smoothness measurements previously computed by a symmetric finite-difference weighted essentially non-oscillatory (WENO) method.[16–18] In theory, shock-confining filtering should substantially alleviate the smearing of shock waves and introduction of spurious oscillations that, respectively, first- and high-order-accurate linear filtering is liable to elicit.

The purpose of this paper is to conduct a preliminary examination of the effects of linear versus shock-confining LES filters on the physical characteristics of highly compressible turbulence. Note that we do *not* conduct any full LES. Rather, we first perform direct numerical simulations (DNS) of three-dimensional compressible isotropic turbulence interacting with a strong normal shock wave, a configuration that we will refer to as shock/isotropic-turbulence interaction (SITI), and observe the true upstream-to-downstream changes in turbulent flow properties across the interaction region. We then filter the DNS flow solutions using various examples of linear and shock-confining filters and compare these new results against the original ones. In Section II, the mechanics and numerical properties of both types of filtering are briefly explained, and in Section III, we describe the tested SITI configurations and direct numerical simulation procedures. Section IV presents the filtering results, and conclusions are drawn in Section V.

II. Shock-Confining Filtering

Define f_i as the value of a spatially varying function $f(x)$ at the grid point x_i, and assume that the filtering operation that transforms the set of functional values $\{f_i\}$ into the set $\left\{\bar{f}_i\right\}$ has compact support, is explicit, and uses a symmetric stencil. Then, for linear (i.e. uniformly applied) filtering,

$$\bar{f}_i = \sum_{n=-N}^{N} a_n \, f_{i+n} \tag{1}$$

in which the coefficients $\{a_n\}$ must sum to one. The continuous Fourier transform of this type of discrete filtering operation is the transfer function

$$\hat{G}(\kappa) = \sum_{n=-N}^{N} a_n \, e^{-in\kappa} \tag{2}$$

in which $i = \sqrt{-1}$ and κ is wavenumber nondimensionalized by grid spacing; and if $a_{-n} = a_{+n}$ for all n, as is usually the case, then

$$\hat{G}(\kappa) = \Re\left\{\hat{G}(\kappa)\right\} = a_0 + 2\sum_{n=1}^{N} a_n \, \cos\left(n\kappa\right) \tag{3}$$

Due to the previously stated requirement that the coefficients $\{a_n\}$ sum to one, $\hat{G}(0) = 1$ identically, indicating that for sinusoidal fluctuations of wavelengths approaching infinity (approximately represented by the length of the computational domain), their amplitudes are neither attenuated nor amplified. In order to minimize commutation error between filtering operations and differentiation, Vasilyev et al.[15] establish that $\hat{G}(\kappa)$ should strike a certain balance between number of zero moments and number of vanishing derivatives at the Nyquist wavenumber $\kappa = \pi$, which is the smallest wavenumber theoretically resolvable by the computational grid. For $N = 1$ (3-point filter), this is best (but not ideally) accomplished by the well-known top-hat filter, in which

$$\begin{pmatrix} a_{-1} \\ a_0 \\ a_{+1} \end{pmatrix} = \frac{1}{4}\begin{pmatrix} 1 \\ 2 \\ 1 \end{pmatrix} \tag{4}$$

and the resulting "cutoff" wavenumber κ^*, defined such that $\hat{G}(\kappa^*) = \frac{1}{2}$, is exactly $\frac{1}{2}\pi$. For $N = 2$ (5-point filter), this is best accomplished by the coefficients

$$\begin{pmatrix} a_{-2} \\ a_{-1} \\ a_0 \\ a_{+1} \\ a_{+2} \end{pmatrix} = \frac{1}{16} \begin{pmatrix} -1 \\ 4 \\ 10 \\ 4 \\ -1 \end{pmatrix} \tag{5}$$

for which $\kappa^* = \arccos\left(1 - \sqrt{2}\right) \simeq \frac{2}{3}\pi$. Finally, for $N = 3$ (7-point filter), this is best accomplished by the coefficients

$$\begin{pmatrix} a_{-3} \\ a_{-2} \\ a_{-1} \\ a_0 \\ a_{+1} \\ a_{+2} \\ a_{+3} \end{pmatrix} = \frac{1}{32} \begin{pmatrix} -1 \\ 0 \\ 9 \\ 16 \\ 9 \\ 0 \\ -1 \end{pmatrix} \tag{6}$$

for which $\kappa^* = \frac{1}{2}\pi$. Figure 1 plots the (real) transfer functions of these three examples.

The shock-confining filtering technique proposed by Grube et al.[14] employs such linear commutative filters as "optimal" components of an adaptive filtering approach that is designed to reduce to these filters, or others like them, in perfectly smooth flow regions. The quantitative degree of local non-smoothness is obtained from the smoothness measurements computed by a symmetric finite-difference WENO method[16–18] and expressed in the form of a normalized nonlinearity index[17,19] NI', which always ranges from zero (perfect smoothness) to one (maximum WENO adaptation). NI' values are associated with the interfaces between grid "cells" rather than with the grid points themselves, and in SCF they serve as "opacity" values $\left\{\alpha_{i+1/2}\right\}$ of conceptual porous barriers that during filtering operations variably impede the cross-flow of information between grid points. If, for example, $\alpha_{i+1/2} = \frac{1}{4}$, 75% of the flow field information from points with positional indices greater than $\left(i + \frac{1}{2}\right)$ will be allowed to contribute to the filtering calculations for points with indices less than $\left(i + \frac{1}{2}\right)$, and 25% of that information will be reflected back to the filtering calculations for the originating points. This mechanism is depicted schematically in Fig. 2. In this way, a hypothetical perfect discontinuity, which would yield a perfectly opaque filtering barrier, would strictly prevent the exchange of information between two very different flow states, but a non-perfect discontinuity or high-wavenumber turbulent fluctuation would gradually and correctly allow increasingly more information to be exchanged as α diminished.

Consider for a moment a 3-point filtering stencil, and define $f'_{i,j}$ as the effective value of $f(x)$, after appropriate shock-confining modifications, at the ith grid point for the purpose of calculating the filtered value $\bar{f}(x)$ at the jth grid point; then

$$\bar{f}_i = a_{-1}\, f'_{i-1,i} + a_0\, f'_{i,i} + a_1\, f'_{i+1,i} \tag{7}$$

In this case, the two relevant grid cell interfaces are those with positional indices $\left(i \pm \frac{1}{2}\right)$, so according to the transmission and reflection paradigm described above,

$$\begin{aligned} f'_{i-1,i} &= \left(1 - \alpha_{i-1/2}\right) f_{i-1} + \alpha_{i-1/2}\, f_i \\ f'_{i,i} &= f_i \\ f'_{i+1,i} &= \left(1 - \alpha_{i+1/2}\right) f_{i+1} + \alpha_{i+1/2}\, f_i \end{aligned} \tag{8}$$

For larger stencil sizes, the effective values assigned to grid points far from the center must incorporate the transmission and reflection fractions of *all* intervening barriers; for example, for a 5-point stencil,

$$\begin{aligned} f'_{i-2,i} &= \left(1 - \alpha_{i-3/2}\right)\left(1 - \alpha_{i-1/2}\right) f_{i-2} + \left[1 - \left(1 - \alpha_{i-3/2}\right)\left(1 - \alpha_{i-1/2}\right)\right] f_i \\ f'_{i+2,i} &= \left(1 - \alpha_{i+3/2}\right)\left(1 - \alpha_{i+1/2}\right) f_{i+2} + \left[1 - \left(1 - \alpha_{i+3/2}\right)\left(1 - \alpha_{i+1/2}\right)\right] f_i \end{aligned} \tag{9}$$

Therefore, for general shock-confining filtering,

$$\bar{f}_i = \sum_{n=-N}^{N} b_{n,i}\, f_{i+n} \tag{10}$$

in which

$$b_{n,i} = \begin{cases} a_n \displaystyle\prod_{k=n+1}^{0} \left(1 - \alpha_{i+k-1/2}\right), & n < 0 \\ a_0 + \displaystyle\sum_{m=n}^{-1} a_m \left[1 - \prod_{k=m+1}^{0} \left(1 - \alpha_{i+k-1/2}\right)\right] + \sum_{m=1}^{n} a_m \left[1 - \prod_{k=0}^{m-1} \left(1 - \alpha_{i+k+1/2}\right)\right], & n = 0 \\ a_n \displaystyle\prod_{k=0}^{n-1} \left(1 - \alpha_{i+k+1/2}\right), & n > 0 \end{cases} \tag{11}$$

This construction satisfies the important mathematical properties that (i) $f(x)$ is globally conserved over the computational domain and (ii) uniform flow regions remain uniform. Additional details regarding the implementation of SCF and the incorporation of WENO smoothness information for multiple flow variables spanning multiple spatial dimensions can be found in Grube et al.[14]

III. Shock/Isotropic-Turbulence Interaction

Decaying three-dimensional isotropic turbulence (IT) is a canonical flow field that realistically represents the small scales of many turbulent flows and, if compressible, can generate shocklets that are strong and numerous enough to require special shock-capturing treatment when investigated numerically. The physics of compressible isotropic turbulence as manifested by direct numerical simulations (DNS) has been studied by Passot and Pouquet,[20] Lee et al.,[21] and Samtaney et al.[22] Convecting isotropic turbulence across a strong normal shock wave leads to shock/isotropic-turbulence interaction (SITI), a more narrowly targeted canonical configuration representative of local interaction regions in configurations such as shock/turbulent-boundary-layer interaction that are of much current engineering interest in the context of supersonic flight. In SITI, shock-capturing numerical treatments must contend not only with fleeting shocklets of most often moderate strength but also a strong, persistent, and semi-fixed main shock region that is nonetheless unsteady to the point of substantially influencing global flow dynamics. Notable DNS of SITI employing *in*compressible isotropic turbulence are the works of Lee et al.[23] and Mahesh et al.,[24] the latter of which is the primary source for the simulation procedure of the current work. No studies employing compressible isotropic turbulence have yet been published.

III.A. General Computational Configuration

Many properties of an SITI configuration are determined by the properties of the separately established IT field that provides inflow turbulence. The appropriate physical domain for this inflow simulation is a three-dimensional cube with periodic boundary conditions and an edge length L that encompasses a sufficiently broad sampling of large-scale turbulence structures; an evenly-spaced Cartesian grid discretizes this domain into N^3 points. For characterizing the flow state, the following two nondimensional parameters are of chief importance: the Reynolds number based on the Taylor microscale

$$Re_\lambda = \frac{\langle\rho\rangle\, u'_{\text{rms}}\, \lambda}{\langle\mu\rangle} \tag{12}$$

in which angled brackets indicate mean quantities, u'_{rms} is the root-mean-squared fluctuating velocity (per component) and λ is the Taylor microscale; and the turbulent Mach number

$$M_t = \frac{q}{\langle a\rangle} \tag{13}$$

in which a is the speed of sound and q is the root-mean-squared fluctuating velocity magnitude. Note that Re_λ and M_t are not constant throughout an IT simulation because the global strength of the turbulent

fluctuations steadily decays over time without external forcing, which we do not include. A randomized solenoidal approximation to isotropic turbulence serves as an initial flow field, and to transform it into realistic turbulence, we evolve this field through a transient period lasting on the order of τ_t, which is the initial state's reference time λ/u'_{rms}. Although Mahesh et al.[24] artificially adjust the resulting IT field so that it conforms to Morkovin's hypothesis before entering the SITI domain, the present work follows Lee et al.[23] and omits this step.

To generate shock/isotropic-turbulence interaction, this single instantaneous realization of isotropic turbulence is convected through the inflow boundary of the SITI configuration at supersonic Mach number M, which constitutes a third governing parameter. Because this inflow is supersonic, the boundary conditions here are completely specified, and no further boundary treatment is necessary. Domain size and resolution in directions perpendicular to the mean flow are determined by the uniform edge length L and grid resolution N of the inflow IT field. Useful domain size parallel to the mean flow, which is chosen to be aligned with the x-axis, is designated L_x and need only be large enough to comfortably contain the corrugations of the main shock that passing turbulence is known to cause. In the current work, $L_x = \frac{1}{2}L$. Within L_x there are N_x grid points in the streamwise direction, which are weakly clustered around the main shock, located at $\frac{1}{2}L_x$, according to the relationship

$$\tilde{x}(\tilde{\imath}) = \frac{\tilde{\imath} - \alpha\, f(\tilde{\imath})}{1 - \alpha} \tag{14}$$

in which $\tilde{\imath} = i/\left(N_x - 1\right)$ and lies in the range $[0, 1]$, $\tilde{x} = x/L_x$, and

$$f(\tilde{\imath}) = \frac{1}{2}\left(1 + \frac{\tanh\left[\beta\left(2\tilde{\imath} - 1\right)\right]}{2\tanh\beta}\right) \tag{15}$$

After interacting with the main shock, the altered turbulence field approaches the outflow boundary at *sub*sonic speed. An untreated subsonic outlet produces artificial acoustic reflections that can improperly influence the upstream flow; therefore, approximately non-reflecting boundary conditions[25] are specified here for the convective terms. As additional insurance, an L_s-wide sponge layer[24,26] designed to damp stray reflections is inserted between the end of the useful domain and the outflow boundary. A sketch of the entire computational domain resulting from all of these arrangements is provided by Fig. 3.

While statistical quantities in isotropic turbulence are globally space-averaged at each point in time, in SITI they are time- and spanwise-averaged at each streamwise location.

III.B. Tested Specific Configurations

We conduct direct numerical simulations that approximate the convective terms of the Navier-Stokes equations with a bandwidth-optimized symmetric WENO scheme[16–18] utilizing four points per candidate stencil; the viscous terms with fourth-order-accurate central differencing; and time advancement with a third-order-accurate low-storage Runge-Kutta scheme[27] and a CFL number of 0.5. The inflow isotropic turbulence field is initialized with nominal Reynolds number $\left(Re_\lambda\right)_0$ and turbulent Mach number $\left(M_t\right)_0$ and then evolved until $t = 1.5\tau_t$, when the IT initialization transient has sufficiently subsided. After we introduce this instantaneous field into the SITI domain at mean convective Mach number M, resetting $t = 0$, we must allow its leading edge to fully propagate across the useful computational domain before initiating the gathering of SITI statistics. This transient period lasts until $t = t^*\tau_t$, in which

$$t^* = \frac{L_x}{2\tau_t}\left(\frac{1}{U_\uparrow} + \frac{1}{U_\downarrow}\right) \tag{16}$$

and $U_\uparrow$ and $U_\downarrow$ indicate mean convective velocities at the inflow (upstream) and outflow (downstream) boundaries, respectively. Because the inflow IT field is periodic in all spatial directions, including the streamwise one, contributions to SITI statistics cease to contain independent information at $t = \left(t^* + t^\circ\right)\tau_t$, in which

$$t^\circ = \frac{L}{\tau_t U_\uparrow} \tag{17}$$

and therefore the gathering of statistics is halted at this time. Table 1 lists grid resolution, grid stretching, statistical sampling, and governing parameters for three tested SITI configurations, in which the inflow turbulence is either incompressible ("I") or compressible ("C").

Figure 4 presents instantaneous contours of density gradient magnitude, normalized by the time- and spanwise-averaged density at each streamwise location, on sample two-dimensional cross-sections of SITI Cases (a) I, (b) C1, and (c) C2. In order to maximize visual contrast, the contour levels are nonlinearly spaced in a manner that is consistent between the three configurations. For Cases I and C1, in which the ratios of inflow turbulent Mach number to convective Mach number are fairly low, the thin region of large density gradient indicative of the main shock position is entirely distinct from the surrounding turbulence; but for Case C2, in which the ratio is much higher, the unsteady shocklets of the inflow isotropic turbulence are often of comparable strength to the main shock, which itself is of highly variable local strength. Additionally, while the main shock of the incompressible case remains quite flat, the main shocks of the two compressible cases become strongly and unsteadily corrugated during the shock/turbulence interaction process. The consequent broadening of the interaction region's spatial extent is clearly apparent in the statistical flow property profiles of Fig. 5, which plots normalized root-mean-squared deviations of (a) kinetic energy and (b) temperature across the streamwise domain. For all three cases, temperature fluctuations temporarily spike across the interaction region and then roughly resume the original upstream decay trajectory; kinetic energy fluctuations, on the other hand, become permanently amplified, decaying downstream from new, stronger baseline conditions. As turbulent Mach number increases, the distance required for these *global* flow adjustments to establish themselves also increases.

IV. Filtering of SITI

IV.A. Procedure

To prepare the direct numerical simulations of shock/isotropic-turbulence interaction described in the previous section for filtering, we first truncate the $\frac{1}{2}N$ instantaneous flow fields sampled and stored at even intervals between t^* and $(t^* + t^\circ)$ so that $\delta = m\Delta$, in which Δ is the original DNS grid spacing and δ is the new LES-appropriate grid spacing. For Case I, we set $m = 4$, and for Cases C1 and C2, we set $m = 5$; both values are the maximum allowable if filter-related boundary effects are to be prevented from encroaching too far into the useful computational domain for all tested stencil sizes. In directions perpendicular to the mean flow, the truncation is designed to be exact (i.e. all new grid points coincide precisely with a subset of old grid points), but in the streamwise direction, it is not generally possible with exact truncation to simultaneously preserve the grid stretching function of Eq. (14) and maintain the physical locations of end- and mid-points. Thus, in the streamwise direction only, we employ linear interpolation between original DNS grid points in order to obtain approximate flow property values at new grid points chosen such that $\delta_x(x) = m\,\Delta_x(x)$, in which the position-dependent streamwise grid spacing is equivalent to the first derivative of Eq. (14), appropriately scaled. After truncating the DNS flow fields in this manner but before proceeding to filtering, we compute and store the WENO nonlinearity indices that will be necessary for the shock-confining filtering procedure.

As described in Section II, the linear filters and the optimal components of the shock-confining filters that are considered in the present work are 3-, 5-, and 7-point instances of a class of commutative filters proposed by Vasilyev et al.[15] The 3-point filter also happens to be equivalent to the well-known top-hat filter. Recall that the cutoff wavenumber of the 3- and 7-point filters is exactly one-half of the Nyquist wavenumber while the cutoff wavenumber of the 5-point filter is roughly two-thirds of the Nyquist wavenumber. Because this disparity significantly affects the division of length scales into resolved scales and those that are relegated to turbulence modeling, we do not expect to encounter consistent trends from three to five to seven points.

IV.B. Results

Streamwise profiles of the root-mean-squared kinetic energy and temperature fluctuations of the filtered flow fields of Case I are displayed in Figs. 6 and 7, respectively, in which Figs. 6(a) and 7(a) show all of the linear filters together and Figs. 6(b) and 7(b) show all of the shock-confining filters together. Concerning the kinetic energy fluctuations, the natural peak indicated by the DNS results across the shock/turbulence interaction region is substantially diminished by each of the linear filters (and more so for smaller stencils); and immediately downstream of this region, where the second derivative of the DNS profile is highly negative, each of the linearly filtered profiles is highly curved in precisely the opposite sense. In contrast, each of the shock-confining filters leads to a fluctuation peak that is both noticeably closer to that of the DNS and not meaningfully different from the peak of any of the other SCFs; and the sign of the second derivative of each

of the associated profiles is properly maintained across the full streamwise domain. Note that the 7-point SCF produces results are virtually indistinguishable from those of the 3-point SCF even though this is not wholly true of the 5-point SCF. Regarding the temperature fluctuations, the application of linear filtering causes the temporary spike across the interaction region to begin much further upstream than that of the DNS; and again the curvature of the downstream profiles becomes qualitatively different after linear filtering. Shock-confining filtering, on the other hand, mitigates these aberrations.

Figures 8 and 9 present the corresponding streamwise profiles of root-mean-squared deviations of kinetic energy and temperature, respectively, for Case C1. Concerning the kinetic energy fluctuations, the small "shoulder" exhibited by the DNS profile on the downstream side of the TKE-amplifying interaction region is entirely absent from each of the linearly filtered profiles; each of the shock-confining filters, however, faithfully captures this feature. As before, the 3- and 7-point SCFs generate coincident profiles, and unlike before, away from the main shock/turbulence interaction region, where turbulence-induced shocklets are in this case relatively few and weak, the 5-point SCF produces results that match those of the 5-point linear filter quite closely. Regarding the temperature fluctuations, the application of linear filtering with larger and larger stencil sizes leads to peak values that increasingly approach the maximum value of the DNS profile and then, under the 7-point filter, even surpass it. This *global* overshooting behavior suggests that in this case the 7-point filter is creating new, artificial temperature extrema that are strong and numerous enough to clearly manifest themselves statistically rather than becoming swallowed by the remainder of the data. In fact, we find that in the streamwise-normal plane associated with this statistical overshoot, at least one grid point among the collection of time samples reveals negative temperature, a catastrophically non-physical condition. As before, after linear filtering the temperature fluctuation spike begins further upstream than it should while the SCFs largely avoid this disparity; and though some of the SCFs appear to severely diminish the magnitude of this spike, this may be an illusion caused by non-optimal grid point placement.

Because the profiles of the root-mean-squared kinetic energy fluctuations of the filtered flow fields of Case C2 do not raise any additional observational points beyond those already reported for Case C1, these plots are omitted. Streamwise profiles of the root-mean-squared temperature fluctuations for this case are shown in Fig. 10, in which Fig. 10(a) displays all of the linear filters together and Fig. 10(b) displays all of the shock-confining filters together. As before, the profiles generated by linear filters of larger and larger stencil sizes exhibit peak values across the broadening interaction region that approach and then exceed that of the DNS profile; furthermore, in this case, global overshooting occurs for, in addition to the 7-point filter, the 5-point filter as well, and again we find that such overshoots correspond to streamwise locations that encompass at least one instance of grossly non-physical negative temperature. The application of shock-confining filters, however, leads to no such deficiencies.

V. Conclusions

Uniformly high-order-accurate filtering of fluid flow properties in the presence of shocks and shocklets is theoretically susceptible to the same problem that afflicts uniformly high-order-accurate numerical methods for approximating the convective terms of the Navier-Stokes equations: the introduction of new, non-physical extrema near discontinuities. For decades, extensive investigations have been conducted into myriad types of shock-capturing methods, which adaptively decrease their order of accuracy within shock-containing regions in order to maintain accuracy and stability over time. Inspired by such work, Grube et al.[14] have proposed the conceptually similar idea of shock-confining filtering, in which examples from a class of commutative linear filters developed by Vasilyev et al.[15] are subject to adaptive adjustment of its filtering coefficients based on previously computed WENO smoothness information. In the current work, we have utilized the turbulent flow fields produced by direct numerical simulations of shock/isotropic-turbulence interaction to perform preliminary *a priori* testing of these shock-confining filters against the corresponding linear filters. Nominal turbulent Mach numbers of the inflowing isotropic turbulence range from 0.2 (incompressible) to 0.7 (moderately compressible) to 1.3 (highly compressible).

According to the original DNS results, normalized root-mean-squared kinetic energy fluctuations, statistically compiled separately at each streamwise location, become permanently amplified from the upstream side of the interaction region to the downstream side. Linear filtering consistently causes this streamwise profile to exhibit qualitative curvature anomalies immediately downstream of the main shock, indicative of non-negligibly altered global flow dynamics, but these can be just as consistently avoided by the alternative application of shock-confining filters. In addition, we observe that the profile of the 7-point SCF, which

incorporates information from the relative grid point range $[-3, 3]$, always precisely coincides with that of the 3-point SCF, which incorporates information from the much smaller range $[-1, 1]$, even though in smooth regions it should be able to access information that the latter cannot possibly reach. This can be explained by the fact that in Eq. (6) the optimal coefficients $a_{\pm 2}$ are exactly zero so that the adapted coefficients $b_{\pm 2}$ in Eq. (11) must also be zero by construction. Thus, if the adaptive coefficients $b_{\pm 3,i}$ are locally forced to be very small by the presence of a discontinuity, the only non-zero coefficients remaining are $b_{\pm 1,i}$ and $b_{0,i}$, which constitute the entirety of the coefficients used by the 3-point SCF. Moreover, Taylor and Martín[28] have demonstrated that the WENO smoothness measurement technique, on which the determination of filtering adaptation is based, is overly sensitive to weak-to-moderate flow field variations; and therefore it is not surprising that the 7-point SCF is rarely permitted to employ its large optimal stencil.

Normalized root-mean-squared temperature fluctuations, according to the original DNS results, temporarily spike across the interaction region. As in the case of the kinetic energy fluctuations described above, linear filtering consistently causes the streamwise profile to exhibit qualitative curvature anomalies immediately downstream of the main shock, anomalies that the use of shock-confining filtering avoids. Additionally, as turbulent Mach number increases, first the 7-point and then both the 5- and 7-point linear filters generate maximum values that exceed the maximum value of the DNS profile; and at the streamwise locations where such overshooting occurs, at least one grid point manifests the catastrophically non-physical attribute of negative temperature. Shock-confining filters, on the other hand, consistently prevent this type of non-physical behavior. In fact, it could be argued that this prevention is actually too effective in that SCF often appears to substantially undercut the proper fluctuation peak, but each of the SCFs performs, according to this measure, at least as well as the 3-point linear filter, so any detrimental consequences may be acceptable. The absence of grossly adverse temperature behavior away from the main shock, coupled with its increasing absence from the interaction region itself as turbulent Mach number decreases, suggests that the shortcomings of linear filtering may be negligible for shocks in relative isolation, becoming important specifically during the interactions of shocks with strong turbulence.

Although the concept of shock-confining filtering requires further study, both *a priori* and *a posteriori*, to verify its necessity and suitability for large-eddy simulations of general compressible turbulence, the results of this preliminary *a priori* investigation indicate that linear filtering can indeed create serious qualitative discrepancies in *global* flow characteristics, discrepancies that are *not* produced by shock-confining filtering. We recommend that linear filters containing coefficients identically equal to zero, such as the 7-point commutative filter, not be employed as the optimal components of SCFs; therefore, of the three shock-confining filters that we have examined in the current study, we especially favor the 5-point SCF for further analysis and development.

Acknowledgments

This work was sponsored by National Science Foundation Grant CTS-0238390 and a National Science Foundation Graduate Research Fellowship. Computational resources were provided by the CRoCCo Laboratory at Princeton University.

References

[1]van Leer, B., "Towards the ultimate conservative difference scheme. V. A second-order sequel to Godunov's method," *Journal of Computational Physics*, Vol. 32, No. 1, 1979, pp. 101–36.

[2]Harten, A., "High resolution schemes for hyperbolic conservation laws," *Journal of Computational Physics*, Vol. 49, No. 3, 1983, pp. 357–93.

[3]Yee, H. C., "Construction of explicit and implicit symmetric TVD schemes and their applications," *Journal of Computational Physics*, Vol. 68, No. 1, 1987, pp. 151–79.

[4]Harten, A., Engquist, B., Osher, S., and Chakravarthy, S. R., "Uniformly high order accurate essentially non-oscillatory schemes, III," *Journal of Computational Physics*, Vol. 71, No. 2, 1987, pp. 231–303.

[5]Shu, C.-W. and Osher, S., "Efficient implementation of essentially non-oscillatory shock-capturing schemes, II," *Journal of Computational Physics*, Vol. 83, No. 1, 1989, pp. 32–78.

[6]Liu, X.-D., Osher, S., and Chan, T., "Weighted essentially non-oscillatory schemes," *Journal of Computational Physics*, Vol. 115, No. 1, 1994, pp. 200–12.

[7]Jiang, G.-S. and Shu, C.-W., "Efficient implementation of weighted ENO schemes," *Journal of Computational Physics*, Vol. 126, No. 1, 1996, pp. 202–28.

[8]Germano, M., Piomelli, U., Moin, P., and Cabot, W. H., "A dynamic subgrid-scale eddy viscosity model," *Physics of Fluids A*, Vol. 3, No. 7, 1991, pp. 1760–5.

[9]Moin, P., Squires, K., Cabot, W., and Lee, S., "A dynamic subgrid-scale model for compressible turbulence and scalar transport," *Physics of Fluids A*, Vol. 3, No. 11, 1991, pp. 2746–57.

[10]Bardina, J., Ferziger, J. H., and Reynolds, W. C., "Improved subgrid-scale models for large-eddy simulation," Paper 1980–1357, American Institute of Aeronautics and Astronautics, 1980.

[11]Speziale, C. G., Erlebacher, G., Zang, T. A., and Hussaini, M. Y., "The subgrid-scale modeling of compressible turbulence," *Physics of Fluids*, Vol. 31, No. 4, 1988, pp. 940–2.

[12]Vreman, B., Geurts, B., and Kuerten, H., "On the formulation of the dynamic mixed subgrid-scale model," *Physics of Fluids*, Vol. 6, No. 12, 1994, pp. 4057–9.

[13]Stolz, S. and Adams, N. A., "An Approximate Deconvolution Procedure for Large-Eddy Simulations," *Physics of Fluids*, Vol. 11, No. 7, 1999, pp. 1699–1701.

[14]Grube, N. E., Taylor, E. M., and Martín, M. P., "Assessment of WENO methods with shock-confining filtering for LES of compressible turbulence," Paper 2007–4198, American Institute of Aeronautics and Astronautics, 2007.

[15]Vasilyev, O. V., Lund, T. S., and Moin, P., "A general class of commutative filters for LES in complex geometries," *Journal of Computational Physics*, Vol. 146, No. 1, 1998, pp. 82–104.

[16]Weirs, V. G. and Candler, G. V., "Optimization of weighted ENO schemes for DNS of compressible turbulence," Paper 1997–1940, American Institute of Aeronautics and Astronautics, 1997.

[17]Weirs, V. G., *A Numerical Method for the Direct Simulation of Compressible Turbulence*, Ph.D. thesis, University of Minnesota, December 1998.

[18]Martín, M. P., Taylor, E. M., Wu, M., and Weirs, V. G., "A bandwidth-optimized WENO scheme for the effective direct numerical simulation of compressible turbulence," *Journal of Computational Physics*, Vol. 220, No. 1, 2006, pp. 270–89.

[19]Taylor, E. M., Wu, M., and Martín, M. P., "Optimization of nonlinear error for weighted essentially non-oscillatory methods in direct numerical simulations of compressible turbulence," *Journal of Computational Physics*, Vol. 223, No. 1, 2007, pp. 384–97.

[20]Passot, T. and Pouquet, A., "Numerical simulation of compressible homogeneous flows in the turbulent regime," *Journal of Fluid Mechanics*, Vol. 181, 1987, pp. 441–66.

[21]Lee, S., Lele, S. K., and Moin, P., "Eddy shocklets in decaying compressible turbulence," *Physics of Fluids A*, Vol. 3, No. 4, 1991, pp. 657–64.

[22]Samtaney, R., Pullin, D. I., and Kosović, B., "Direct numerical simulation of decaying compressible turbulence and shocklet statistics," *Physics of Fluids*, Vol. 13, No. 5, 2001, pp. 1415–30.

[23]Lee, S., Lele, S. K., and Moin, P., "Interaction of isotropic turbulence with shock waves: Effect of shock strength," *Journal of Fluid Mechanics*, Vol. 340, 1997, pp. 225–47.

[24]Mahesh, K., Lele, S. K., and Moin, P., "The influence of entropy fluctuations on the interaction of turbulence with a shock wave," *Journal of Fluid Mechanics*, Vol. 334, 1997, pp. 353–79.

[25]Thompson, K. W., "Time dependent boundary conditions for hyperbolic systems," *Journal of Computational Physics*, Vol. 68, No. 1, 1987, pp. 1–24.

[26]Israeli, M. and Orszag, S. A., "Approximation of radiation boundary conditions," *Journal of Computational Physics*, Vol. 41, No. 1, 1981, pp. 115–35.

[27]Williamson, J. H., "Low-storage Runge-Kutta schemes," *Journal of Computational Physics*, Vol. 35, No. 1, 1980, pp. 48–56.

[28]Taylor, E. M. and Martín, M. P., "Stencil adaptation properties of a WENO scheme in direct numerical simulations of compressible turbulence," *SIAM Journal on Scientific Computing*, Vol. 30, No. 3, 2007, pp. 533–54.

Case	M	$(Re_\lambda)_0$	$(M_t)_0$	$(Re_\lambda)_\uparrow$	$(M_t)_\uparrow$	$(Re_\lambda)_\downarrow$	$(M_t)_\downarrow$
I	1.5	25	0.2	15.5	0.135	17.3	0.113
C1	2.0	35	0.7	27.6	0.569	22.9	0.327
C2	2.0	35	1.3	19.7	0.942	15.4	0.386

Case	N^2	N_x	N_s	t^*	t°	α	β
I	96^2	48	12	0.69	0.97	$\frac{1}{4}$	$\frac{7}{2}$
C1	160^2	80	20	3.20	3.50	$\frac{1}{8}$	3
C2	160^2	80	20	5.55	6.05	$\frac{1}{8}$	2

Table 1. Physical and computational parameters for direct numerical simulations of tested shock/isotropic-turbulence interaction configurations.

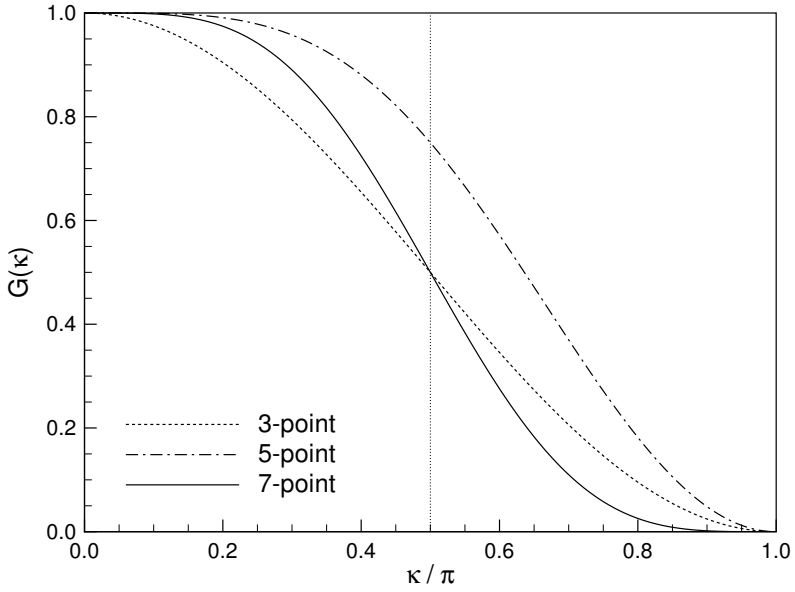

Figure 1. Transfer functions (Fourier transforms) of 3-, 5-, and 7-point commutative linear filters.

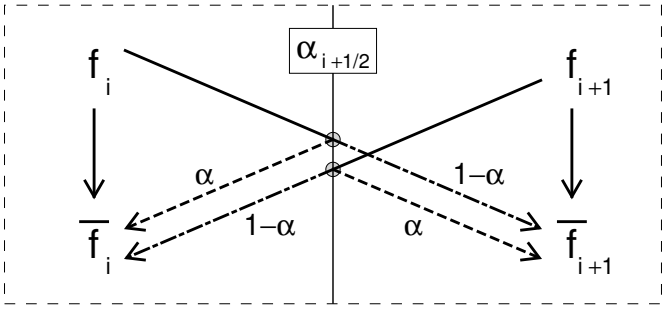

Figure 2. Conceptual transmission and reflection of information during shock-confining filtering at an interfacial porous barrier of "opacity" α governed by local smoothness.

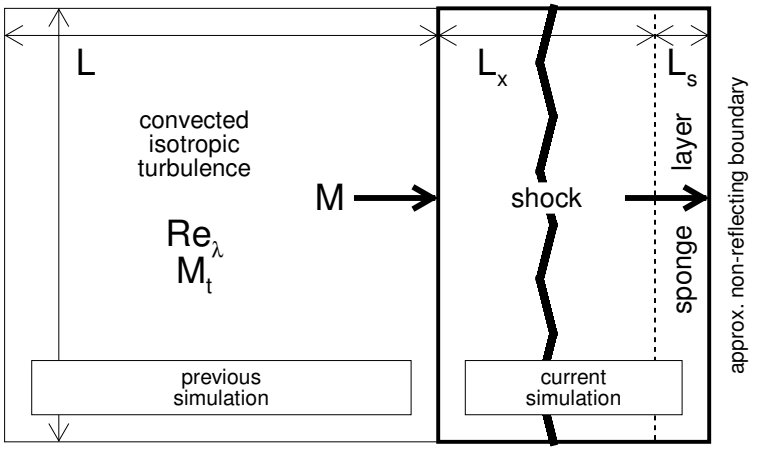

Figure 3. Computational domain sketch for shock/isotropic-turbulence interaction.

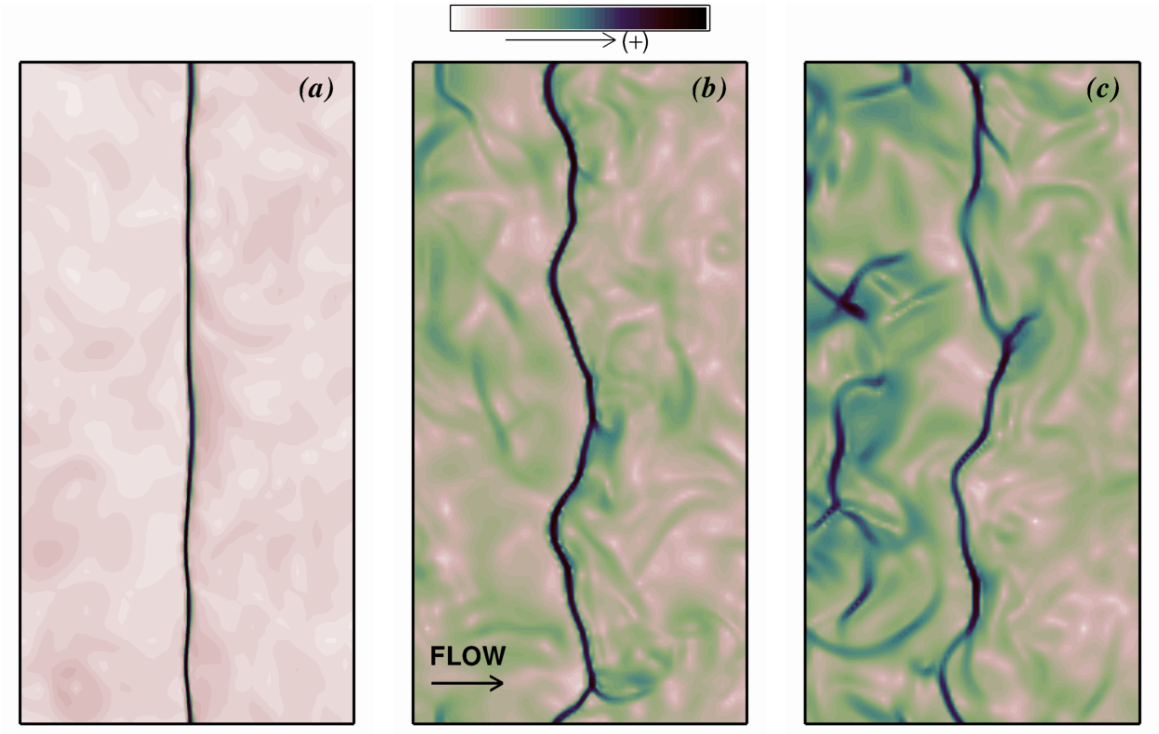

Figure 4. Contours of normalized density gradient $|\nabla\rho| \,/\, \langle\rho\rangle$ on instantaneous cross-sections of DNS of tested shock/isotropic-turbulence interaction configurations. Statistical quantities are time- and spanwise-averaged at each streamwise location. ***(a)*** **Case I.** ***(b)*** **Case C1.** ***(c)*** **Case C2.**

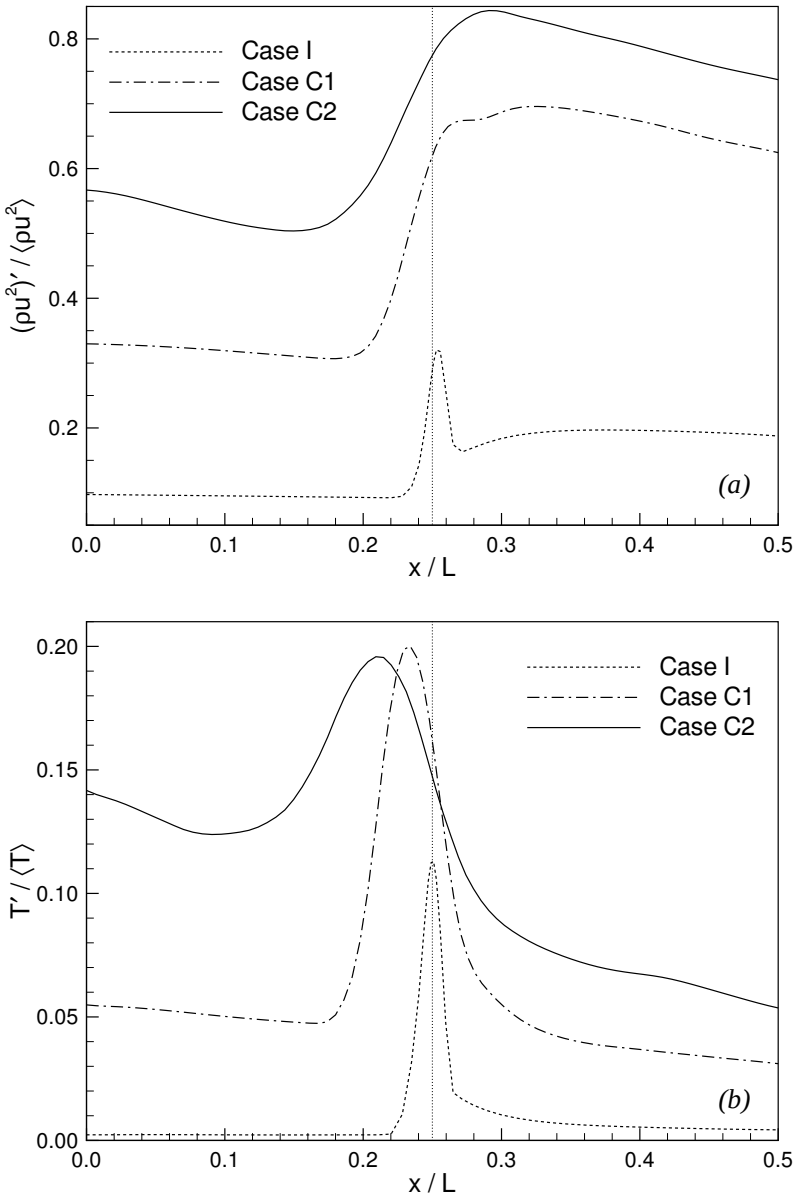

Figure 5. Streamwise profiles of normalized root-mean-squared fluctuations of *(a)* kinetic energy and *(b)* temperature for DNS of tested shock/isotropic-turbulence interaction configurations. Statistical quantities are time- and spanwise-averaged at each streamwise location.

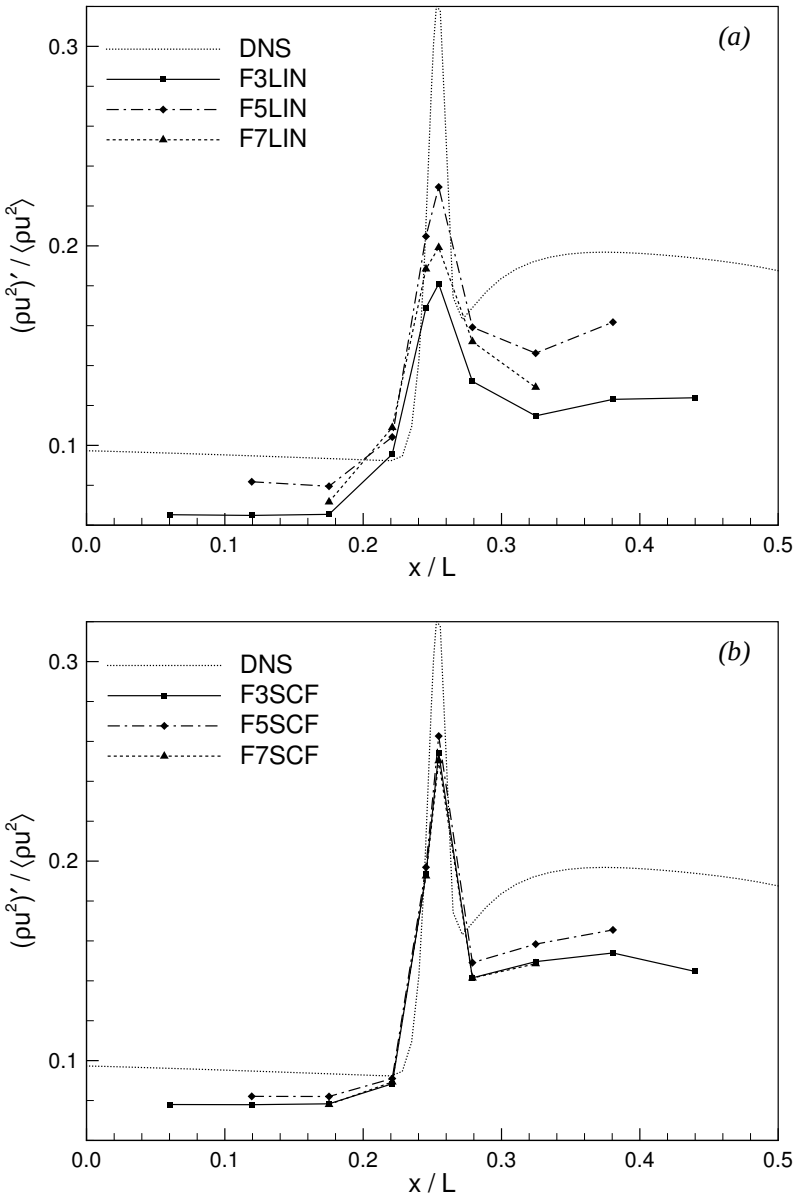

Figure 6. Streamwise profiles of normalized root-mean-squared kinetic energy fluctuations for SITI Case I after truncation and filtering of the DNS flow solution with 3-, 5-, and 7-point commutative filters. *(a)* **Linear filtering.** *(b)* **Shock-confining filtering.**

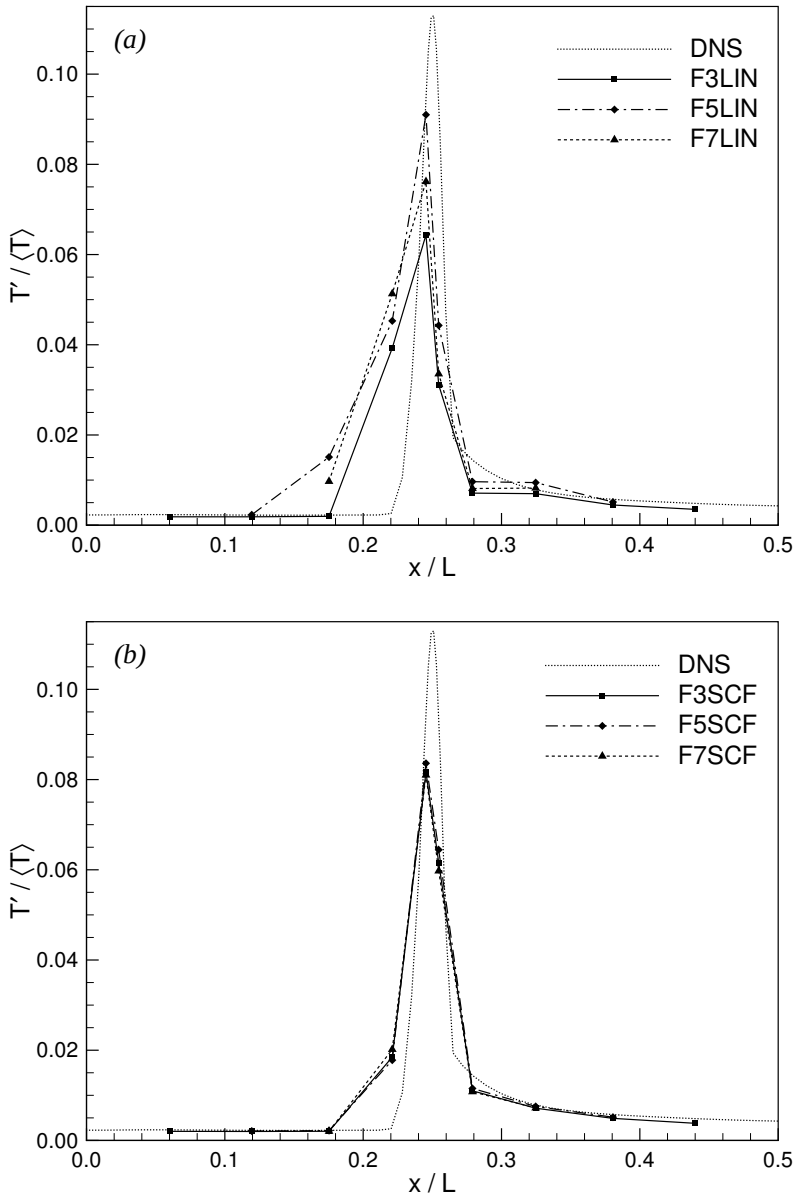

Figure 7. Streamwise profiles of normalized root-mean-squared temperature fluctuations for SITI Case I after truncation and filtering of the DNS flow solution with 3-, 5-, and 7-point commutative filters. *(a)* **Linear filtering.** *(b)* **Shock-confining filtering.**

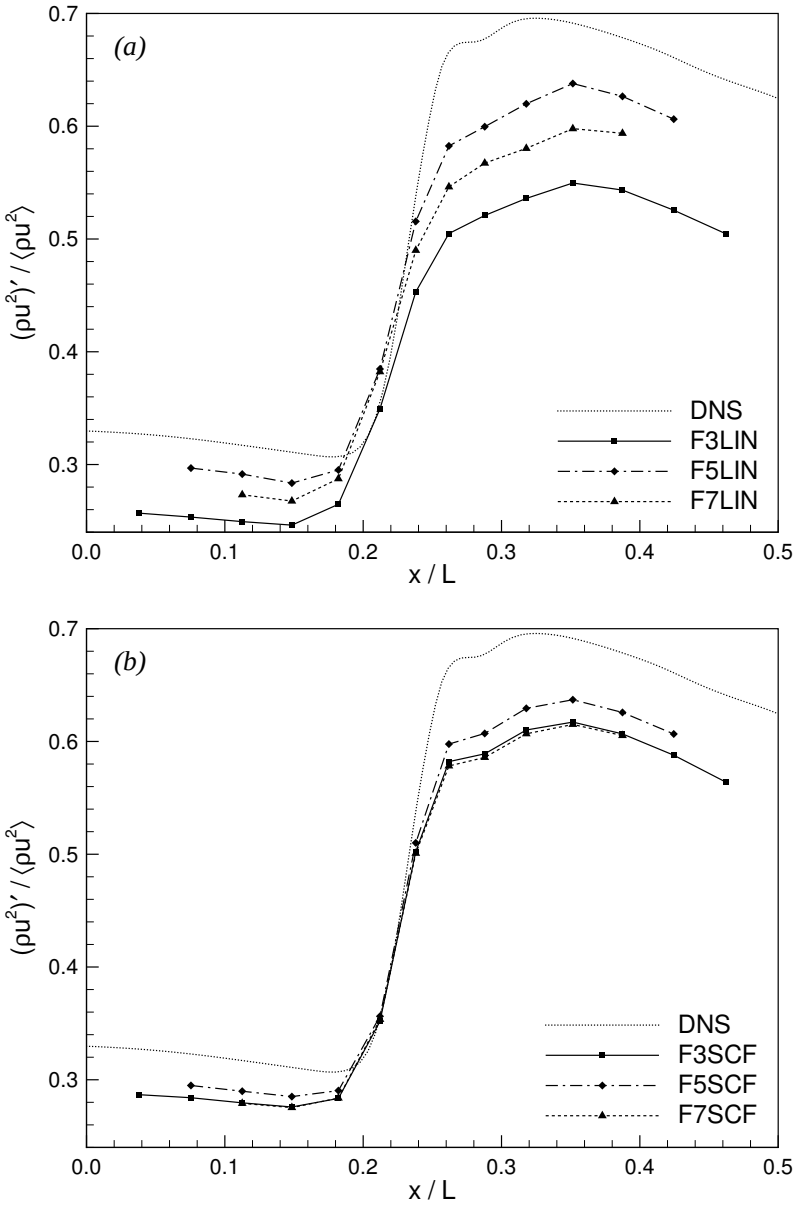

Figure 8. Streamwise profiles of normalized root-mean-squared kinetic energy fluctuations for SITI Case C1 after truncation and filtering of the DNS flow solution with 3-, 5-, and 7-point commutative filters. *(a)* **Linear filtering.** *(b)* **Shock-confining filtering.**

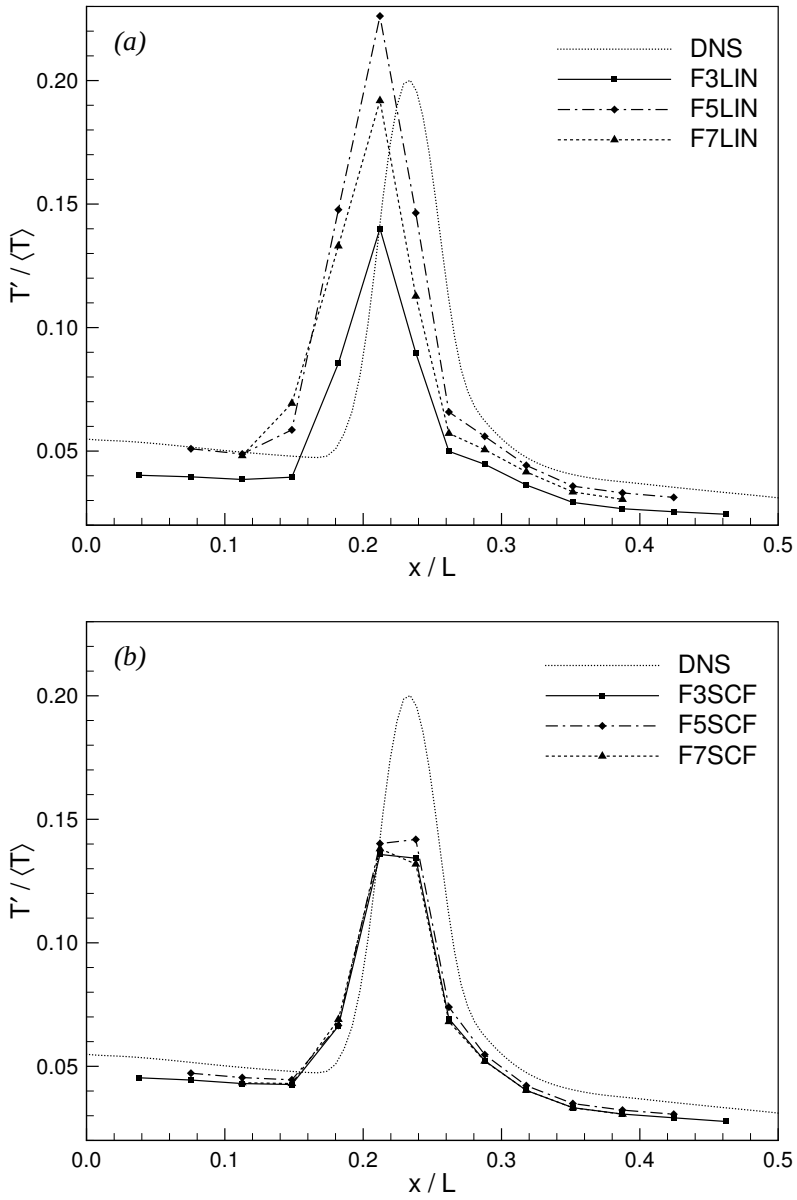

Figure 9. Streamwise profiles of normalized root-mean-squared temperature fluctuations for SITI Case C1 after truncation and filtering of the DNS flow solution with 3-, 5-, and 7-point commutative filters. *(a)* **Linear filtering.** *(b)* **Shock-confining filtering.**

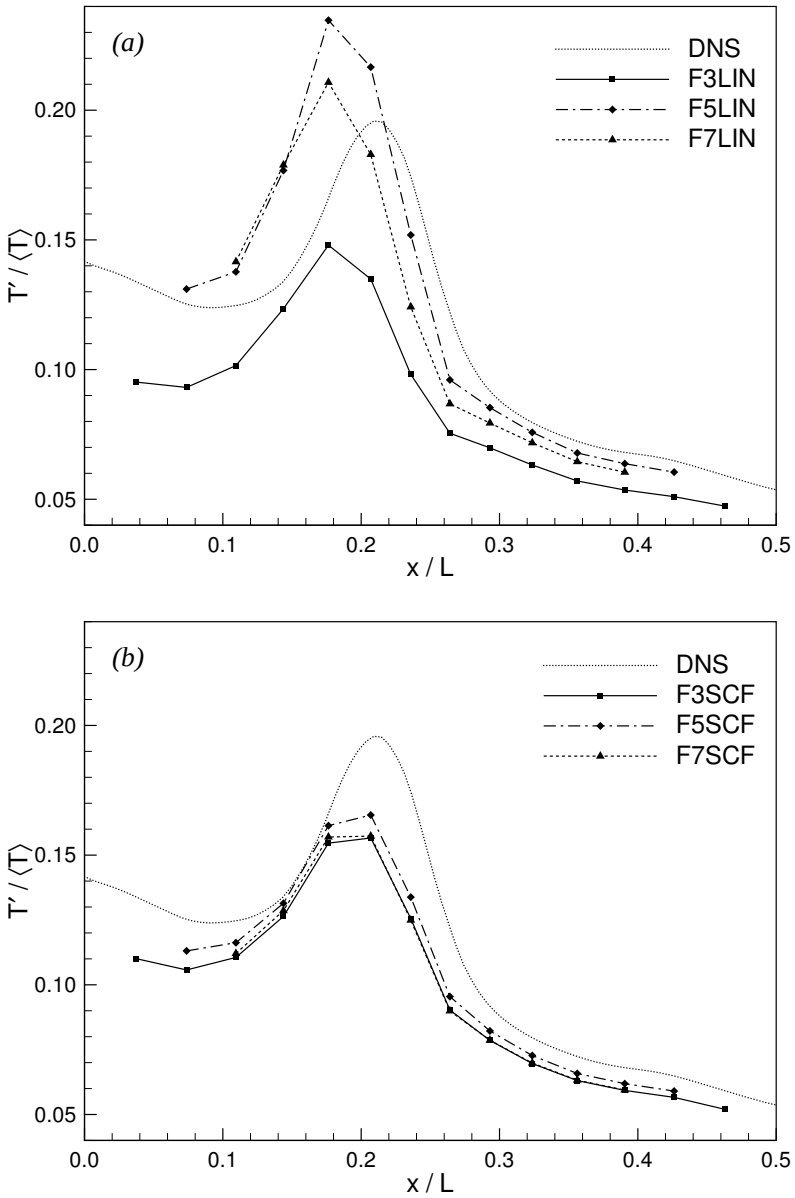

Figure 10. Streamwise profiles of normalized root-mean-squared temperature fluctuations for SITI Case C2 after truncation and filtering of the DNS flow solution with 3-, 5-, and 7-point commutative filters. *(a)* **Linear filtering.** *(b)* **Shock-confining filtering.**